Pérez-Consuegra, N., Hoke, G.D., Fitzgerald, P., Mora, A., Sobel, E.R., and Glodny, J., 2021, Late Miocene–Pliocene onset of fluvial incision of the Cauca River Canyon in the Northern Andes: GSA Bulletin, https://doi.org/10.1130/B36047.1.

Supplemental Material

Figures S1–S12

Table S1. Thermal history model input table for the Cauca River Canyon (Colombia)

Table S2. Compiled thermochronology ages

SUPPLEMENTAL MATERIALS

This supporting information contains two tables and one data set that are cited in the main manuscript. The data provided in the data sets is the information on the new AFT data, including fission track counts and track lengths (Data Set S1). Table S1 contains a summary table with the information required to reproduce the inverse thermal history models. Table S2. Contains the compiled thermochronology ages used in the manuscript figures.

Below we provide details on some of the thermochronology methods and AFT radial plots as well as track length histograms for the 10 bedrock samples and 1 detrital sample.

Finally, we provide a plot of slope versus area for the Cauca River to complement the geomorphology analyses presented in the main text.

1. Heavy mineral separation

Standard heavy liquid and magnetic methods were used to separate apatite (density = 3.1–3.2 g/cm^3) crystals from the bedrock samples. Bedrock samples were crushed, milled and sieved to obtain the 63–250 m fraction. The sieved fraction from each sample was hydraulically sorted on a Wilfley table to separate light minerals from the heavy mineral fraction. The heavier fraction was processed in a Frantz LB-1 magnetic separator using 0.5, 0.8, 1.1 and 1.3 A currents. The non-magnetic fraction after the 1.3 A run was processed for density separation using the heavy liquid Tetrabromoethane (TBE, density = 2.9 g/cm^3) and subsequently using Diiodomethane (MI, density = 3.3 g/cm^3).

2. (U-Th-Sm)/He thermochronology methodology

Apatite grains were handpicked, measured, photographed and packed in 1 mm Pt tubes using an Leica M165 C stereo microscope following the procedure suggested by Farley (2002). The selected apatites were clear grains without apparent inclusions and other impurities. The grain dimensions and numbers of terminations were used to calculate the F_T correction factor (Farley et al., 1996). An ASI Alphachron He extraction and analysis system was used to degas the apatite samples. Blank tubes and age standards (Durango apatite) were routinely run together with samples. Samples were heated by the laser system at 8 A (~3.5W) for 5 min to release all He from the apatite crystals. The amounts of ^{4}He in the purified gas were determined by isotope dilution using a ^{3}He tracer, calibrated against a manometrically determined ^{4}He standard. Each

grain underwent a “re-extract” to ensure the grain was degassed entirely in the first step. After the helium extraction, the samples were prepared for analysis of U, Th, and Sm by isotope dilution at the clean laboratory at GFZ Potsdam using a Thermo Element 2 XR ICP-MS equipped with a CETAC ASX-520 auto-sampler system. Please refer to Zhou et al. (2017) for additional analytical details.

For each analysis we report a weighted error which weights the uncertainty of the isotopic abundance by the relative contribution to the total helium production and also includes the uncertainty on the blank-corrected measured ^{4}He. We report concentrations based on measured abundances and a mass calculated from grain dimensions converted to an equivalent spherical radius (ESR) and an assumed apatite density of 3.15 g/cm^{3}. Single-grain ages were calculated following Meesters and Dunai (2005) using U, Th, Sm atomic abundances, blank-corrected He abundances, the F_T correction factor and the alpha particle stopping distance (Ketcham et al., 2011).

3. Details of thermal history modeling in Hefty

Inverse thermal modeling is a valuable tool to convert thermochronologic data into interpretable information and it is crucial to include information on modeling inputs and parameters so others may evaluate and reproduce the results (Ketcham, 2005). The Table S1 lists criteria used following recommendations by Flowers et al. (2015). Modeling was carried in HeFTy v1.9.3 (Ketcham et al., 2007).

Sample 070118-08

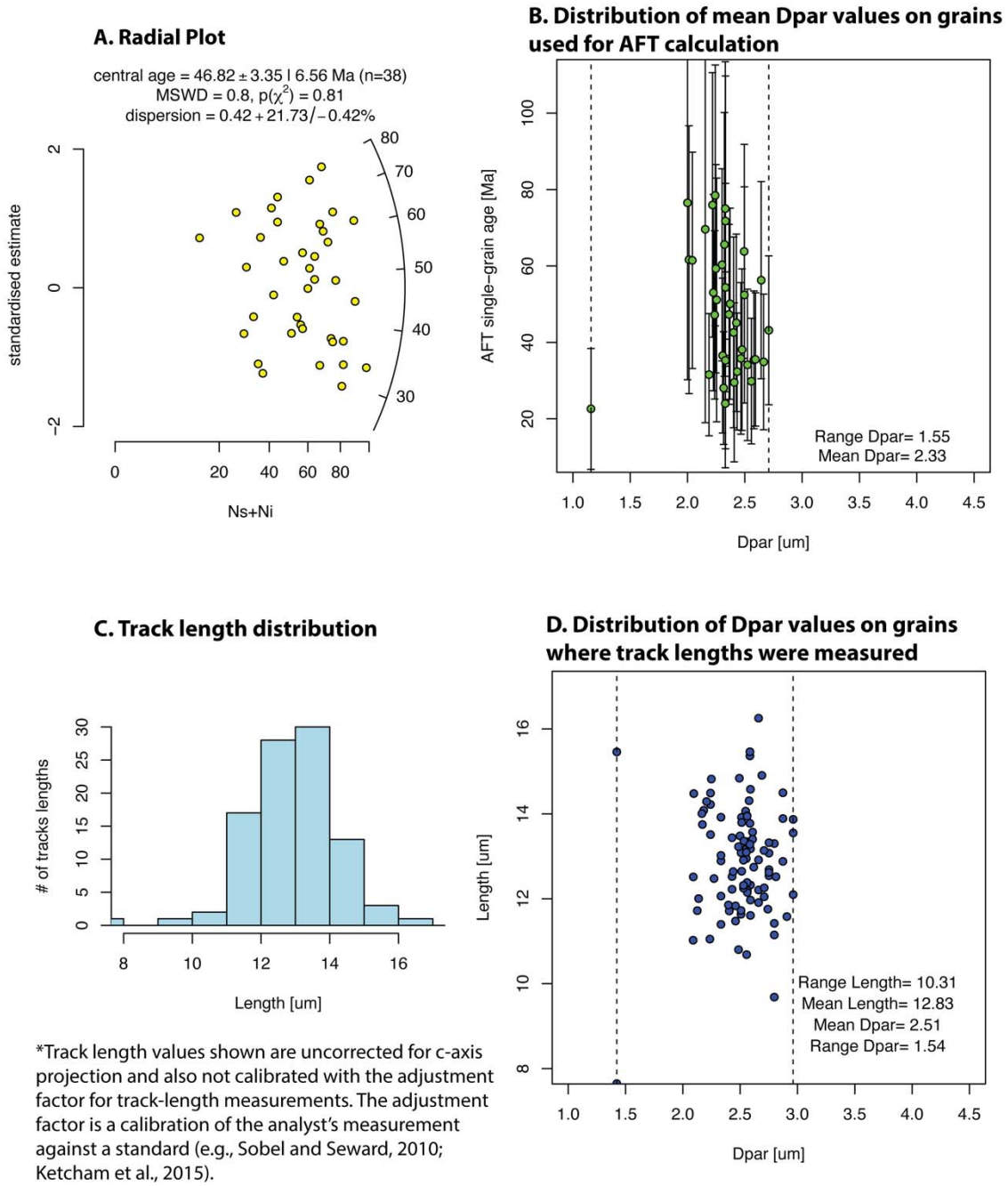

*Track length values shown are uncorrected for c-axis projection and also not calibrated with the adjustment factor for track-length measurements. The adjustment factor is a calibration of the analyst's measurement against a standard (e.g., Sobel and Seward, 2010; Ketcham et al., 2015).

Figure S1.

Sample 0601818-02

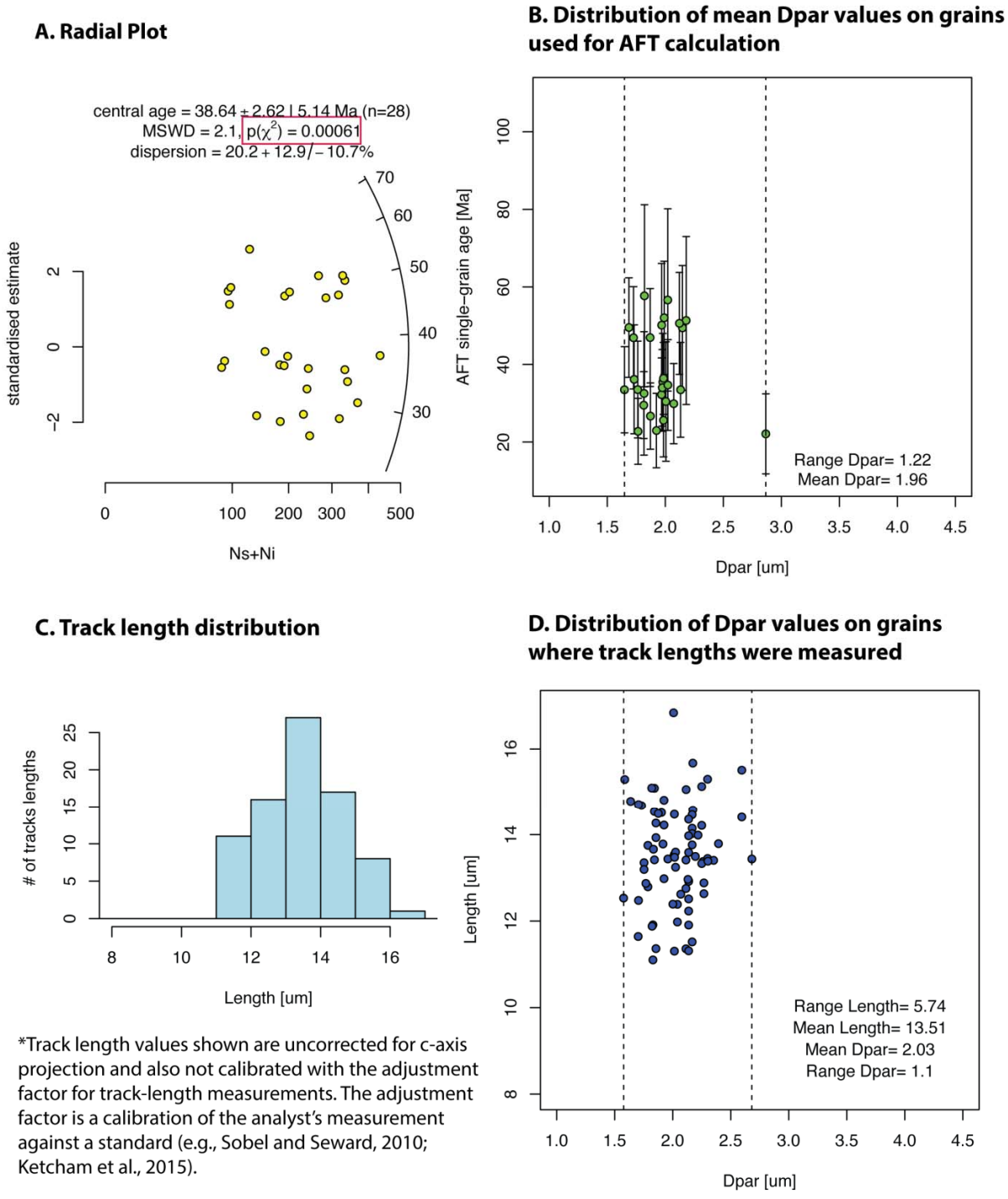

*Track length values shown are uncorrected for c-axis projection and also not calibrated with the adjustment factor for track-length measurements. The adjustment factor is a calibration of the analyst's measurement against a standard (e.g., Sobel and Seward, 2010; Ketcham et al., 2015).

Figure S2.

Sample 0601818-03

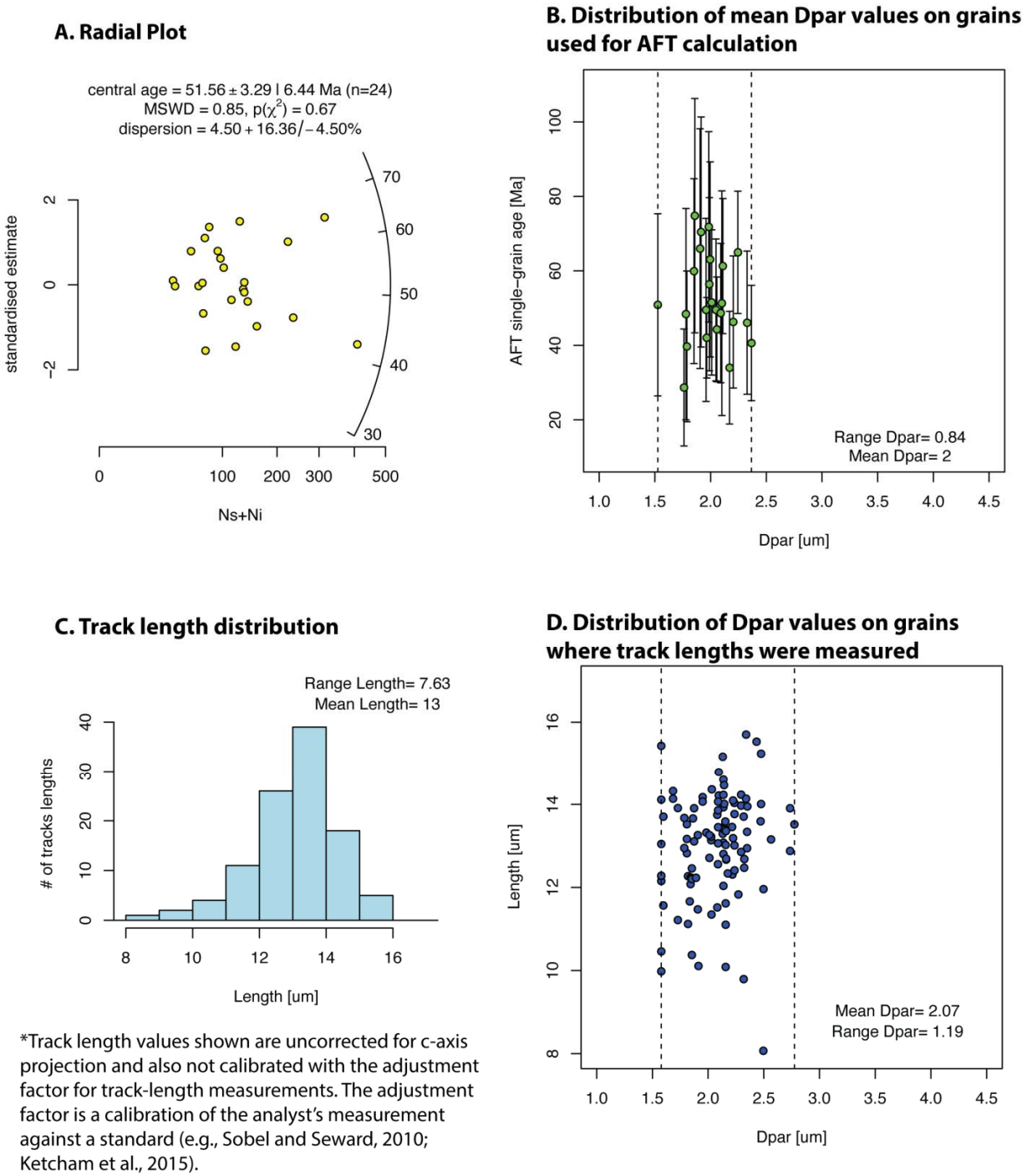

*Track length values shown are uncorrected for c-axis projection and also not calibrated with the adjustment factor for track-length measurements. The adjustment factor is a calibration of the analyst's measurement against a standard (e.g., Sobel and Seward, 2010; Ketcham et al., 2015).

Figure S3.

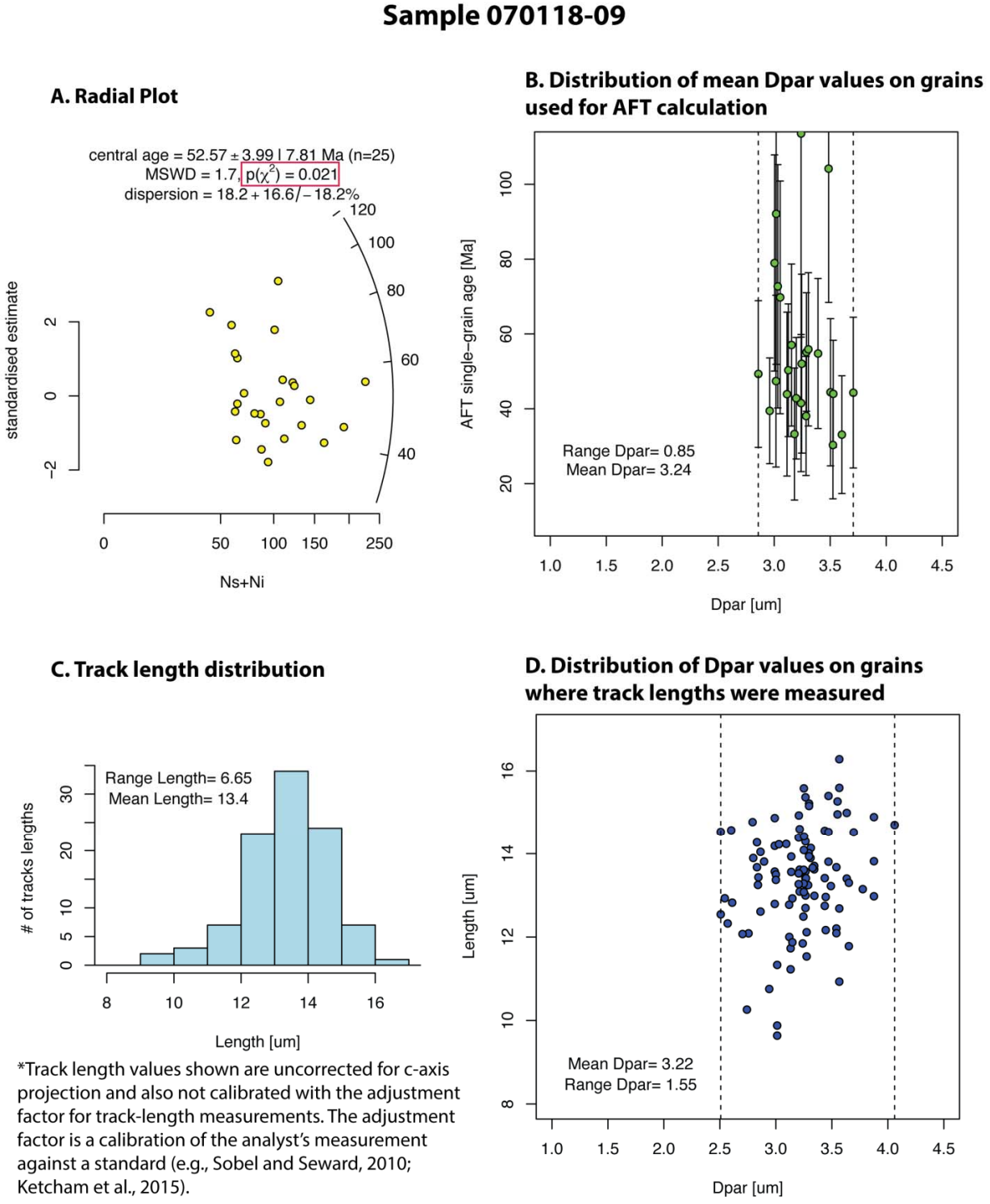

*Track length values shown are uncorrected for c-axis projection and also not calibrated with the adjustment factor for track-length measurements. The adjustment factor is a calibration of the analyst's measurement against a standard (e.g., Sobel and Seward, 2010; Ketcham et al., 2015).

Figure S4.

Sample 070118-07

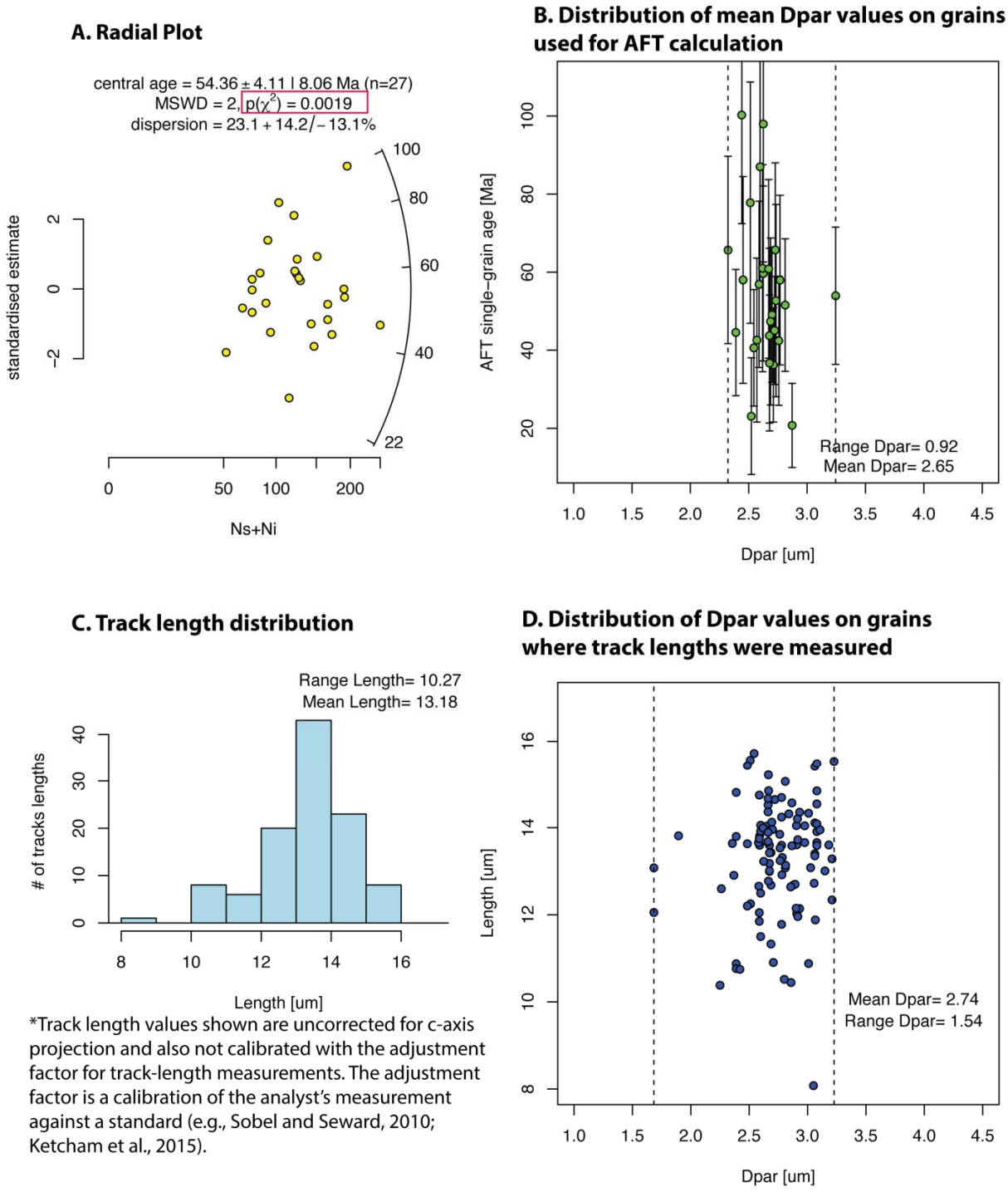

*Track length values shown are uncorrected for c-axis projection and also not calibrated with the adjustment factor for track-length measurements. The adjustment factor is a calibration of the analyst's measurement against a standard (e.g., Sobel and Seward, 2010; Ketcham et al., 2015).

Figure S5.

Sample 070118-05

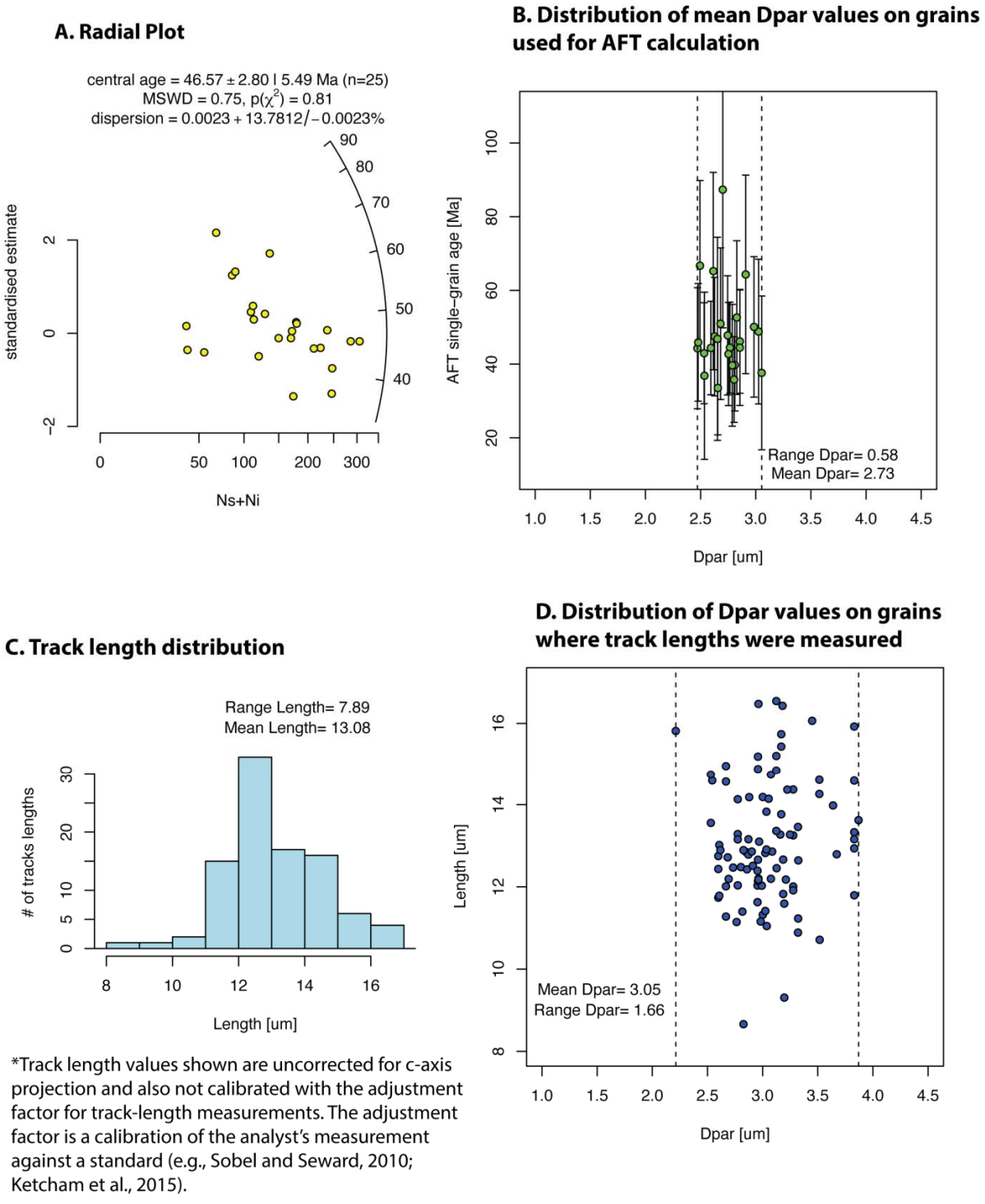

*Track length values shown are uncorrected for c-axis projection and also not calibrated with the adjustment factor for track-length measurements. The adjustment factor is a calibration of the analyst's measurement against a standard (e.g., Sobel and Seward, 2010; Ketcham et al., 2015).

Figure S6.

Sample 070118-04

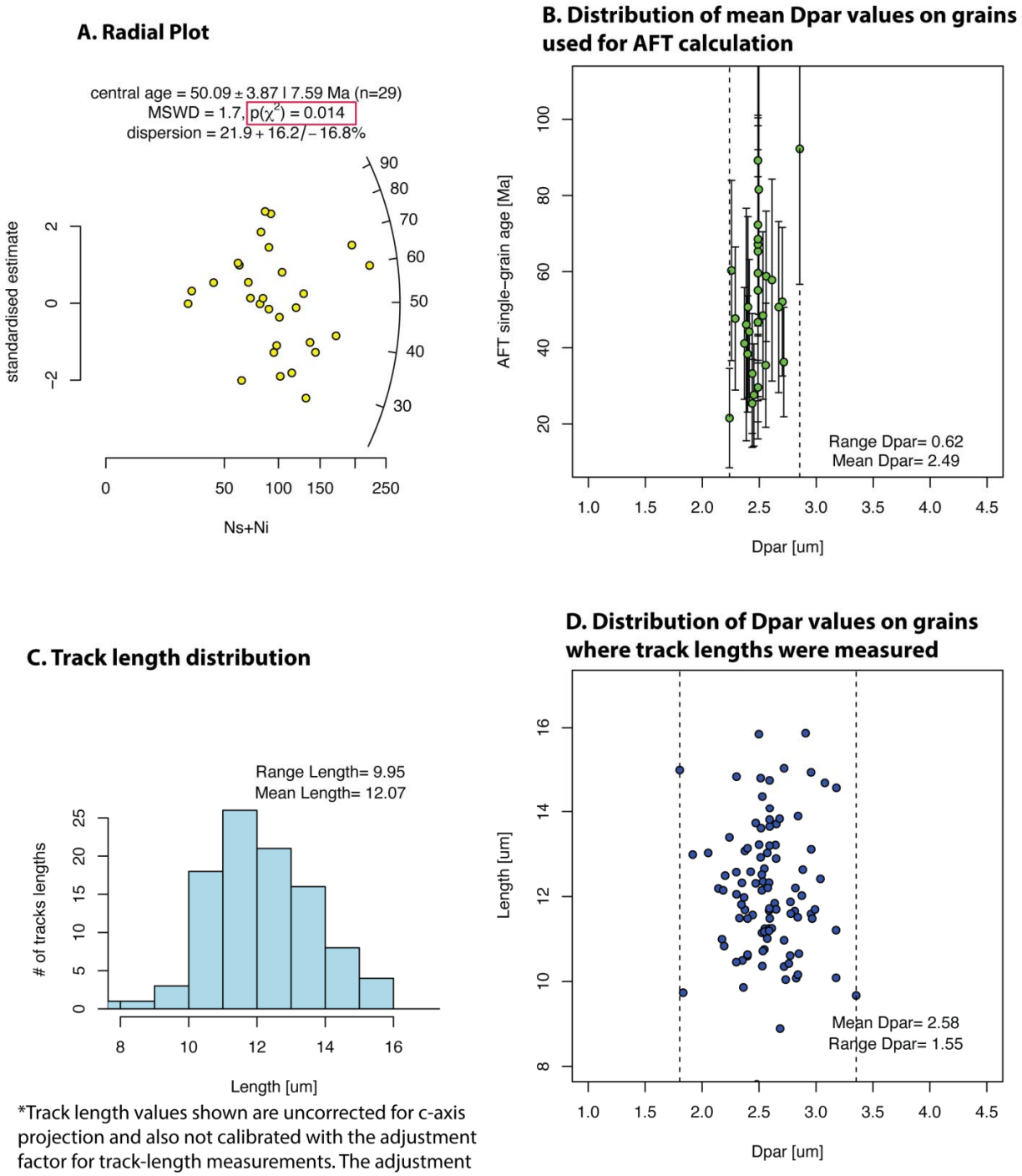

*Track length values shown are uncorrected for c-axis projection and also not calibrated with the adjustment factor for track-length measurements. The adjustment factor is a calibration of the analyst's measurement against a standard (e.g., Sobel and Seward, 2010; Ketcham et al., 2015).

Figure S7.

Sample 267

A. Radial Plot

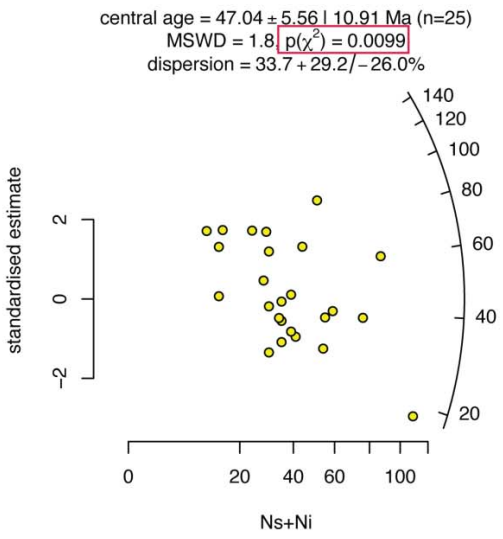

B. Distribution of mean Dpar values on grains used for AFT calculation

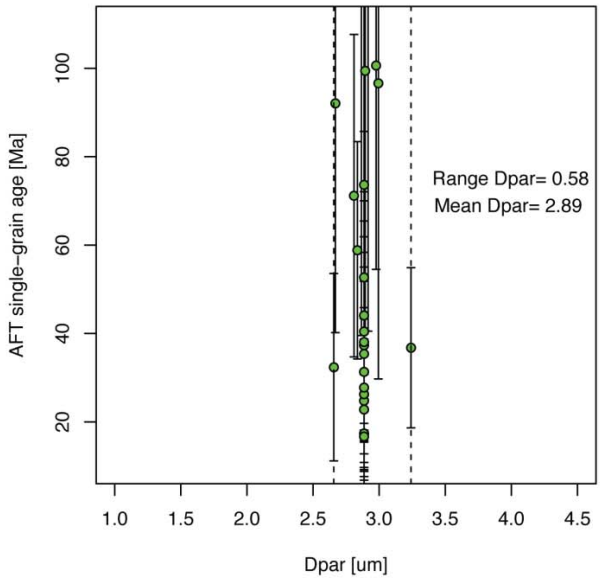

C. Track length distribution

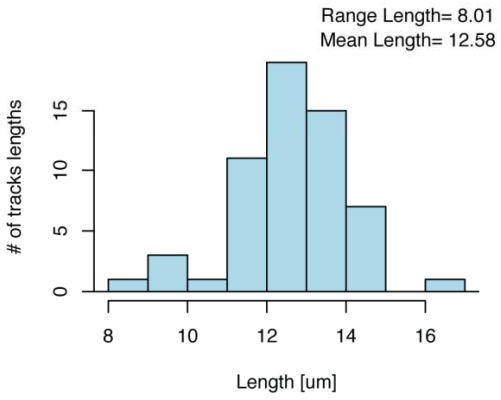

*Track length values shown are uncorrected for c-axis projection and also not calibrated with the adjustment factor for track-length measurements. The adjustment factor is a calibration of the analyst's measurement against a standard (e.g., Sobel and Seward, 2010; Ketcham et al., 2015).

D. Distribution of Dpar values on grains where track lengths were measured

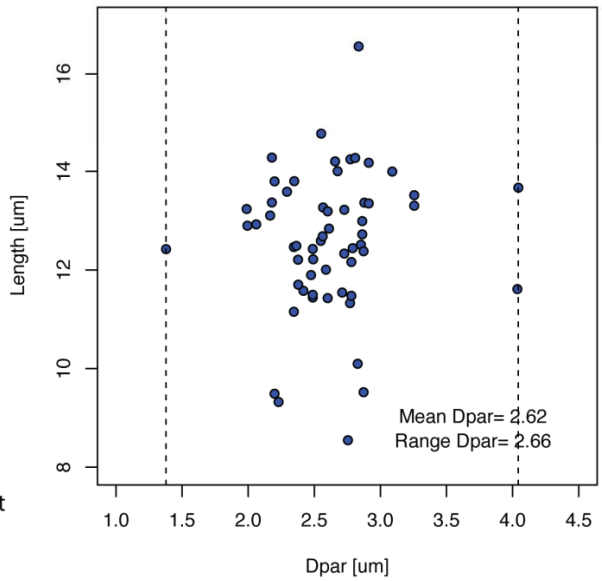

Figure S8.

Sample 274

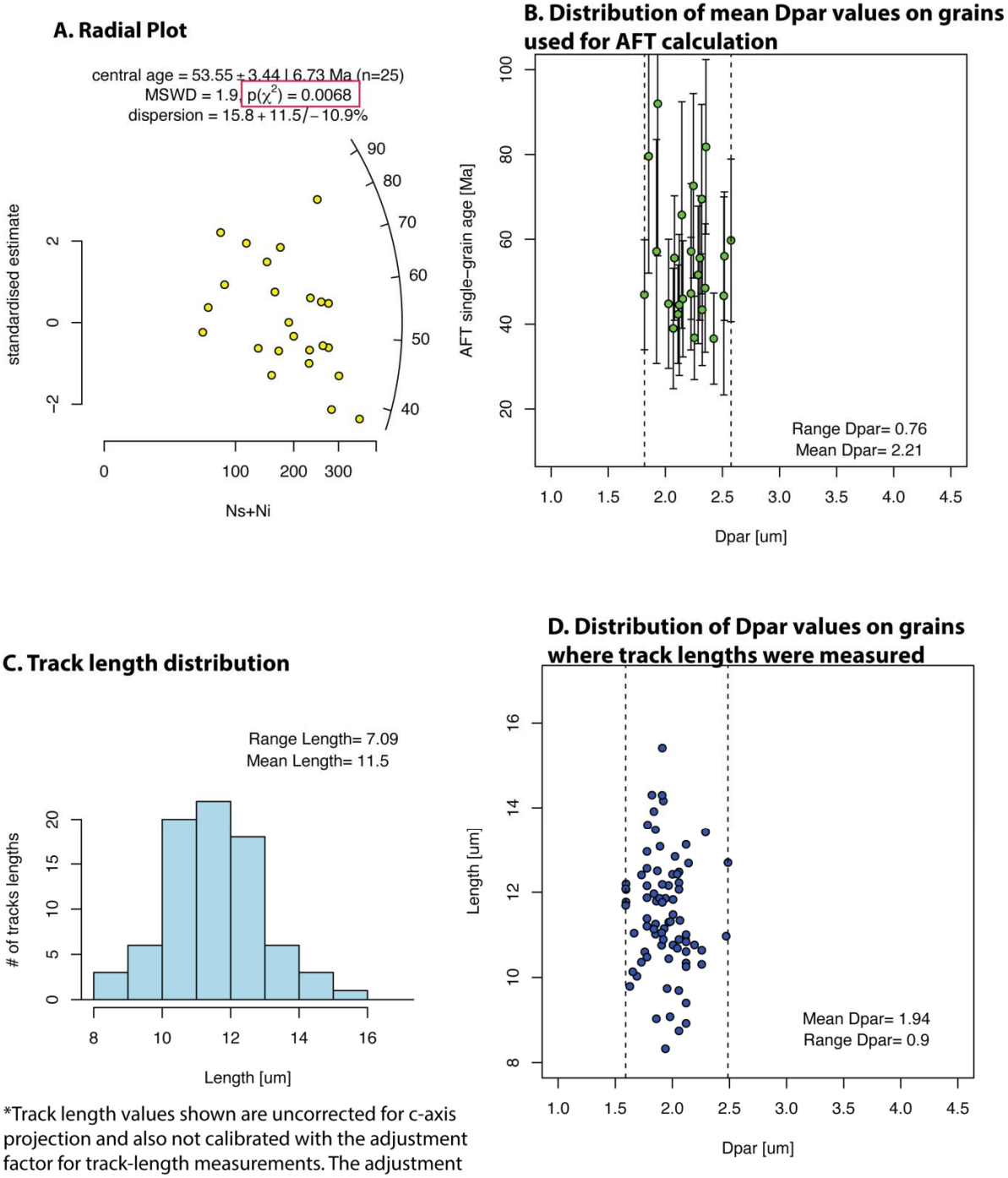

*Track length values shown are uncorrected for c-axis projection and also not calibrated with the adjustment factor for track-length measurements. The adjustment factor is a calibration of the analyst's measurement against a standard (e.g., Sobel and Seward, 2010; Ketcham et al., 2015).

Figure S9.

Sample 273

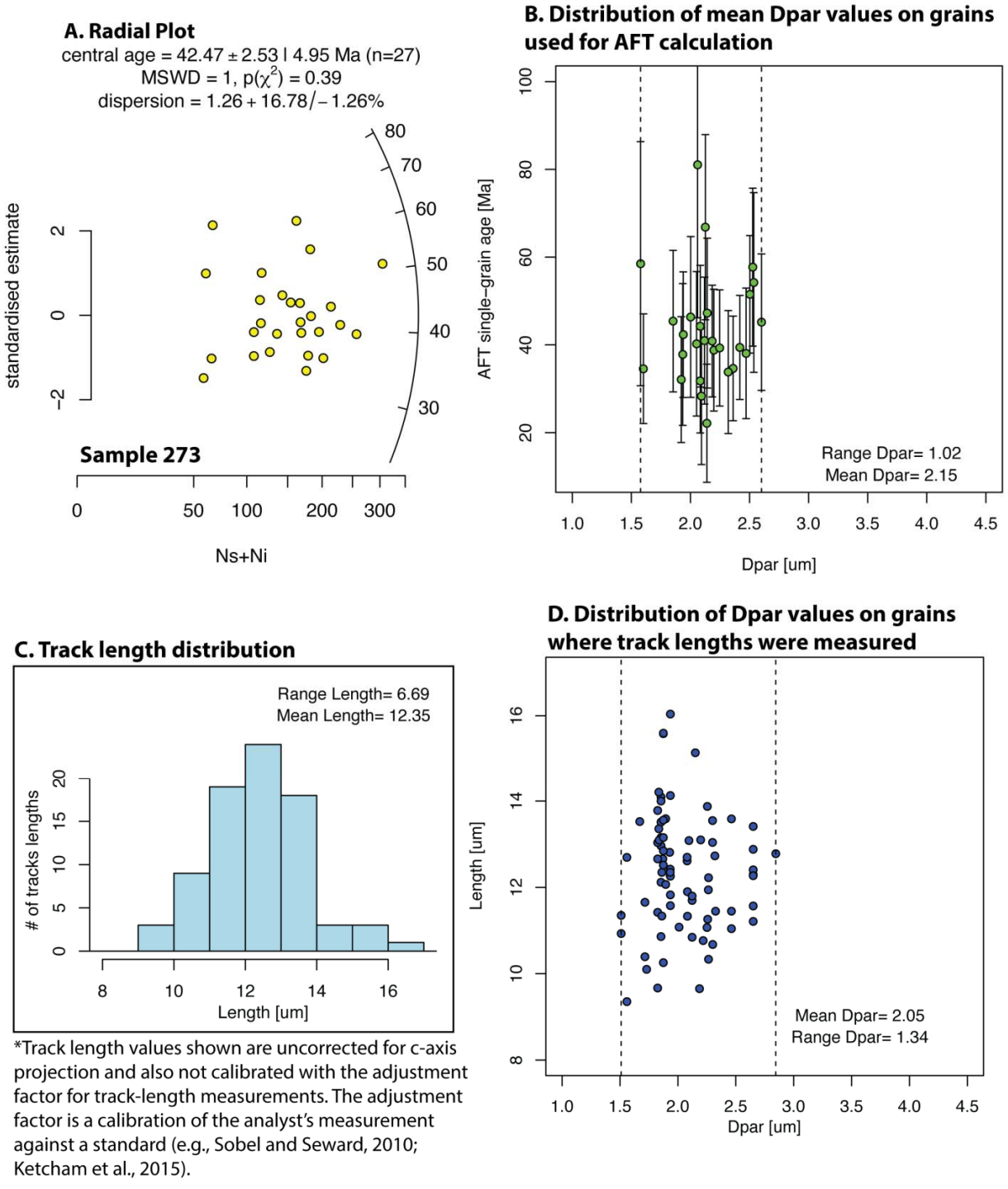

*Track length values shown are uncorrected for c-axis projection and also not calibrated with the adjustment factor for track-length measurements. The adjustment factor is a calibration of the analyst's measurement against a standard (e.g., Sobel and Seward, 2010; Ketcham et al., 2015).

Figure S10.

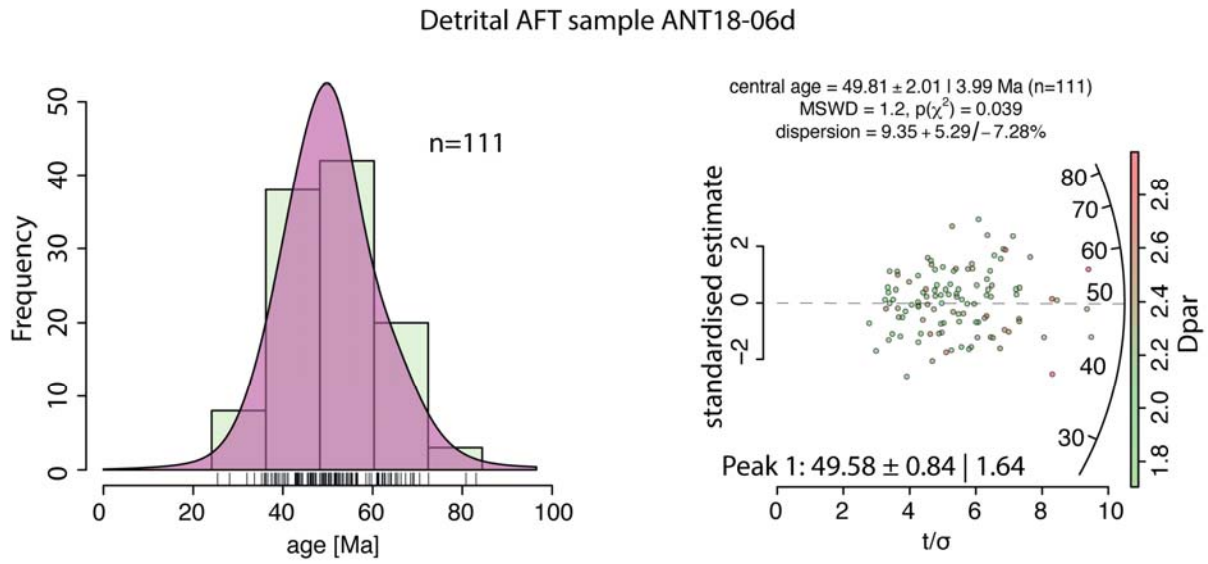
Detrital AFT sample ANT18-06d
n=111
Frequency
age [Ma]
central age = 49.81 ± 2.01 | 3.99 Ma (n=111)
MSWD = 1.2, p(χ²) = 0.039
dispersion = 9.35 + 5.29/−7.28%
standardised estimate
Peak 1: 49.58 ± 0.84 | 1.64
t/σ
Dpar

Figure S11.

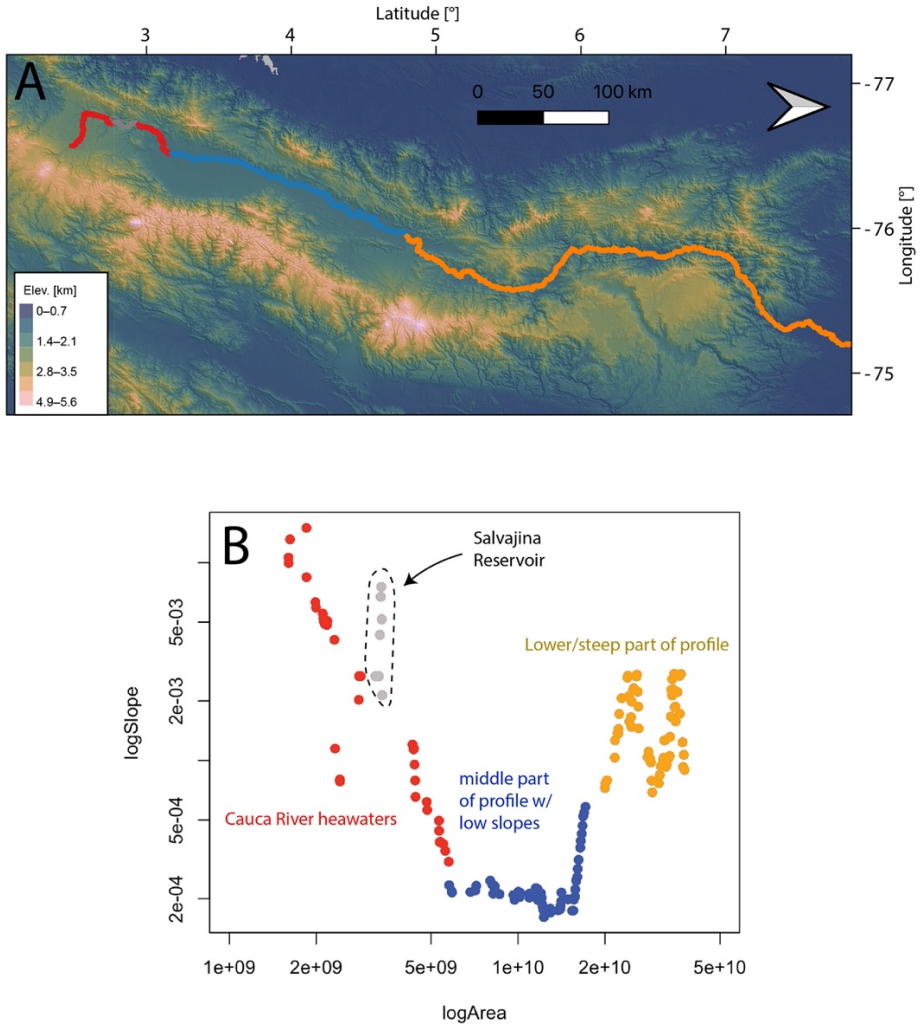

Figure S12. Slope-area relationship for the Cauca River. A. DEM showing the Cauca River profile. B. log-log plot of Slope versus Area color coded according to regions in the Cauca profile.

REFERENCES CITED

[[Not cited?]]Dunai, T.J., González López, G.A., and Juez-Larré, J., 2005, Oligocene-Miocene age of aridity in the Atacama Desert revealed by exposure dating of erosion-sensitive landforms: Geology, v. 33, p. 321–324, https://doi.org/10.1130/G21184.1.

Farley, K.A., 2002, (U-Th)/He Dating: Techniques, Calibrations, and Applications: Reviews in Mineralogy and Geochemistry, v. 47, p. 819–844, https://doi.org/10.2138/rmg.2002.47.18.

Farley, K.A., Wolf, R.A., and Silver, L.T., 1996, The effects of long alpha-stopping distances on (U-Th)/He ages: Geochimica et Cosmochimica Acta, https://doi.org/10.1016/S0016-7037(96)00193-7.

Flowers, R.M., Farley, K.A., and Ketcham, R.A., 2015, A reporting protocol for thermochronologic modeling illustrated with data from the Grand Canyon: Earth and Planetary Science Letters, v. 432, p. 425–435, https://doi.org/10.1016/j.epsl.2015.09.053.

Ketcham, R.A., 2005, Forward and Inverse Modeling of Low-Temperature Thermochronometry Data: Reviews in Mineralogy and Geochemistry, v. 58, p. 275–314, https://doi.org/10.2138/rmg.2005.58.11.

Ketcham, R.A., Carter, A., Donelick, R.A., Barbarand, J., and Hurford, A.J., 2007, Improved measurement of fission-track annealing in apatite using c-axis projection: The American Mineralogist, v. 92, p. 789–798, https://doi.org/10.2138/am.2007.2280.

[[Added from main text.]]Ketcham, R.A., Gautheron, C., and Tassan-Got, L., 2011, Accounting for long alpha-particle stopping distances in (U-Th-Sm)/He geochronology: Refinement of the baseline case: Geochimica et Cosmochimica Acta, v. 75, p. 7779–7791, https://doi.org/10.1016/j.gca.2011.10.011.

Zhou, R., Schoenbohm, L.M., Sobel, E.R., Davis, D.W., and Glodny, J., 2017, New constraints on orogenic models of the southern Central Andean Plateau: Cenozoic basin evolution and bedrock exhumation: Geological Society of America Bulletin, v. 129, p. 152–170, https://doi.org/10.1130/B31384.1.